



UNIVERSITÀ POLITECNICA DELLE MARCHE  
Repository ISTITUZIONALE

Bond of GFRP strips on modern and historic brickwork masonry

This is the peer reviewed version of the following article:

*Original*

Bond of GFRP strips on modern and historic brickwork masonry / Capozucca, Roberto; Ricci, V.. - In: COMPOSITE STRUCTURES. - ISSN 0263-8223. - STAMPA. - 140:(2016), pp. 540-555.  
[10.1016/j.compstruct.2015.12.047]

*Availability:*

This version is available at: 11566/230112 since: 2022-05-25T16:29:33Z

*Publisher:*

*Published*

DOI:10.1016/j.compstruct.2015.12.047

*Terms of use:*

The terms and conditions for the reuse of this version of the manuscript are specified in the publishing policy. The use of copyrighted works requires the consent of the rights' holder (author or publisher). Works made available under a Creative Commons license or a Publisher's custom-made license can be used according to the terms and conditions contained therein. See editor's website for further information and terms and conditions.

This item was downloaded from IRIS Università Politecnica delle Marche (<https://iris.univpm.it>). When citing, please refer to the published version.

(Article begins on next page)

# **Bond of GFRP strips on modern and historic brickwork masonry**

by

R. Capozucca<sup>1</sup> and V. Ricci<sup>2</sup>

## **Abstract**

External bonding strengthening (EBS) of masonry walls with fiber reinforced polymers (FRPs) has become a common technique to improve the mechanical capacity of masonry. In particular, glass fiber reinforced polymer (GFRP) strips are usually adopted as EBS to improve shear capacity under in-plane loading of historic masonry walls in monumental buildings located in seismic areas. Reliability of bond between FRPs and the surface of brickwork walls is condition of adequate strengthening; delamination of FRPs on masonry surface is the mechanism that leads to loss of shear capacity of walls.

In this paper the results of an investigation on the bond between GFRP strips and masonry surface both with modern and historic brickwork masonry are presented. Pull-push shear tests on bonded GFRP-to-brickwork masonry wallets were carried out considering the effects of mortar bed joints having different thicknesses. The experimental results indicated brittle failure due to delamination of GFRP strips; results were processed to evaluate failure load values, strain vs. anchorage length diagrams, shear stress vs. slip relationships experimentally and, energy fracture values. Finally, experimental results are compared with theoretical data obtained from theoretical models.

**Keywords:** Glass-FRP; historic/modern brickwork masonry; pull-push tests; delamination.

---

<sup>1</sup> Confirmed Assoc. Prof. of Structural Engineering, Structural Section DICEA, University Politecnica delle Marche, Ancona, Italy, +39.071.2204570 fax +39.071.2204576 [r.capozucca@univpm.it](mailto:r.capozucca@univpm.it)

<sup>2</sup> Post Graduate student, DICEA, University Politecnica delle Marche, Ancona, Italy.

## 1. INTRODUCTION

Fibre reinforced polymers (FRPs) as external bonded strengthening (EBS) of unreinforced brickwork masonry has increased rapidly as a common technique to strengthen masonry walls often damaged by seismic actions. The preservation of the architectural monumental buildings and common masonry buildings of historic centres represents one of the most important challenges in civil engineering with many aspects such as the complexity of structures' geometry variables related to the materials used and the loading history of such buildings. EBS by FRP strips or sheets are used as a technique for strengthening shear masonry walls [1], increasing the tensile capacity to support combined compression and shear actions set-off during earthquakes [2,3]. Furthermore, FRPs bonded on masonry walls allows increasing collapse displacements significantly [4,5] although the failure due to detachment of FRP on masonry surface may carry to a brittle failure under loading in-plane [6]. Recently, new Codes of Practice have been proposed to define the main rules to follow during the restoration and strengthening of masonry walls [7]. It is well known that for strengthening with bonded FRPs, stress transfers between the composite materials and the surface of the structure [8] with adequate bond strength. Experimental and theoretical works on the bond strength of FRP to concrete element joints have been carried using several set-ups and single shear tests [9-11].

Many theoretical studies on the bond between FRPs and concrete elements have been developed including both fracture mechanics analysis and empirical models [12,13]. In particular, the debonding of FRP-plates on the tensile concrete surface of reinforced concrete beams has been analyzed [14]. In [15,16] the main analytical models present in literature regarding adhesively bonded joints, particularly describe single lap joints; the main parameters considered being the type of adhesive (brittle or ductile), the type of adherent (isotropic with and without yielding, and composites), the overlap length, and the adhesive thickness. An analytical method is shown in [17] to define experimental shear stress vs displacement law in a joint.

Unfortunately, few experimental tests have been developed on the behavior of masonry strengthened by FRP which aim at investigating the delamination of composite FRP materials [18-22]. Strengthened shear walls may show different failure modes which can occur in combination: cracking of masonry in tension, crushing of masonry in compression, shear-sliding of masonry, failure of fiber-reinforced composites and, finally, delamination of FRP from masonry [18,19]. Experimental tests indicate that the dangerous mechanism of brittle failure is due to delamination, especially if the FRP strips are glued to historic clay bricks with a weak clay surface [20,21], taking in account the effects of mortar joints [22]. Furthermore, theoretical analysis with modelling has recently been developed with useful results [23,24]. The delamination of FRP strips or sheets has such a relevant influence on the safety of the strengthening of masonry shear walls that it is useful to investigate the bond strength of FRP-to-brickwork masonry considering both modern and historic masonry walls with different thicknesses of mortar joints. The results of the behavior of glass FRP-to-brickwork wallets composed of historic bricks and of modern full clay bricks experimentally studied by pull-push shear tests are investigated in this paper. The investigation was developed also taking into account the width of bed mortar joints from 4mm thin mortar joints to large joints measuring 12mm. The experimental data were processed to evaluate: shear-slip laws of the specimens tested; energy fracture and failure load values. Furthermore, a theoretical model is shown in the following section to analyze the bond behavior of Glass-FRP-to-brickwork wallets considering neglecting shear lag model [12,25,26]. Finally, modes of failure of Glass-FRP-to-brickwork wallets are discussed and experimental data are compared with analytical results.

## **2. BOND ANALYSIS**

Experimental investigations suggest that the main failure mode of FRP-to-masonry joints is delamination failure under shear generally occurring at a plane located a few millimetres from the surface of the masonry and not on the adhesive interface. A very important aspect of the behaviour

of bonded joints is that an effective bond length exists beyond which the ultimate load cannot be increased by an extension of the bond length. This is a fundamental difference between an EBS and an internal strengthening using rods for which a sufficiently long anchorage length can always be found and the full tensile strength of the reinforcement achieved [18]. The ultimate load of EBS with GFRP strips depends strongly on the fracture energy,  $G_f$ , which can be evaluated by shear stress-slip laws. The following presents a theoretical analysis to predict bond capacity of EBS by GFRP-strips on brickwork masonry considering a simplified elastic model [26].

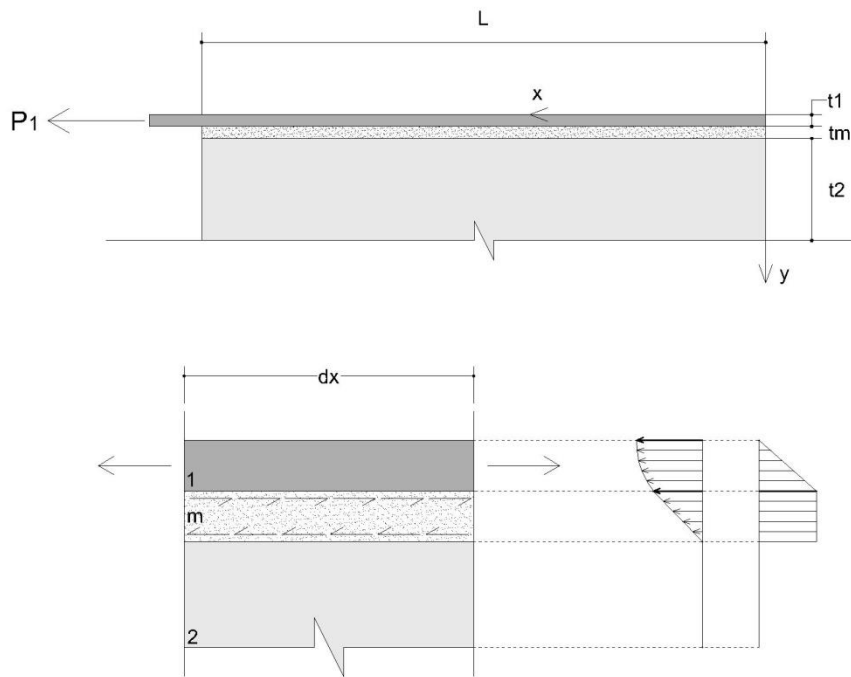


Figure 1 - (a) Specimen of GFRP strip-to-brickwork masonry bonded joint under pull-push test and (b) adherents with displacement and shear stress distribution.

Figure 1(a) shows a scheme of a pull-push shear test of a GFRP strip-to-brickwork masonry bonded joint. The GFRP strip is the *adherent 1* subjected to axial and shear deformations; historic or modern clay brick is the *adherent 2* and a porosity clay layer filled with polymer adhesive is an *ideal intermediate element* “m” subjected to a constant shear stress across its thickness  $t_m$ . The width, thickness, Young’s modulus and shear modulus of the intermediate layer are denoted by  $b_m$ ,  $t_m$ ,  $E_m$  and  $G_m$ , respectively. The *adherent 1* and *ideal intermediate element* are supposed of elastic material. Figure 1(b) shows a differential element  $dx$  with shear stress distribution  $\tau_1(x, y)$  and

displacement function  $u_1(x,y)$  through the thicknesses  $t_1$  and  $t_m$ . The shear stress,  $\tau_a$ , is assumed constant along the whole thickness  $t_m$  of *ideal intermediate element*. For a generic section, the value of the force resulting from the internal normal stresses along  $dy$ , considering a depth equal to one unit of the *adherent 1*, can be written as:

$$P_1(x) = \int_0^{t_1} \sigma_1 \cdot dy \quad (1)$$

The equilibrium of *adherent 1* along the section  $dx$  is given by:

$$\int_0^{t_1} \sigma_1 \cdot b_1 \cdot dy + \tau_a(x) \cdot b_1 \cdot dx - \int_0^{t_1} (\sigma_1 + d\sigma_1) \cdot b_1 \cdot dy = 0 \quad (2)$$

From Eq. (2):

$$\tau_a(x) \cdot dx - \int_0^{t_1} d\sigma_1 \cdot dy = 0 \quad (3)$$

Considering Eq. (1) and differentiating by  $x$ , we obtain:

$$dP_1(x) = \int_0^{t_1} d\sigma_1 \cdot dy \quad (4)$$

Introducing Eq. (4) in Eq.(3), the following differential equation can be obtained:

$$\frac{dP_1}{dx} - \tau_a(x) = 0 \quad (5)$$

Furthermore, shear stress along the *adherent 1* is given by:

$$\tau_1(x, y) = \frac{\tau_a(x)}{t_1} \cdot y \quad (6)$$

with the shear strain equal to:

$$\gamma_1(x, y) = \frac{\tau_a}{G_1 \cdot t_1} \cdot y \quad (7)$$

Assuming negligible shear strain  $\gamma_1(x, y) \cong 0$  in the *adherent 1*, along the whole thickness  $t_1$ , the following displacement function:

$$u_1(x, y) = u_{1,top}(x) - \int_0^y \gamma_1(x, y) \cdot dy \quad (8)$$

can be simplified as:

$$u_1(x, y) \cong u_1(x) \cong u_{1,top}(x) \cong u_{1,bottom}(x) \quad (9)$$

From Eq. (1), it is:

$$P_1(x) = \int_0^{t_1} E_1 \cdot \frac{du_1(x, y)}{dx} \cdot dy \cong E_1 \cdot \frac{du_1(x)}{dx} \cdot t_1 \quad (10)$$

Taking into account Eq. (5), it can be written:

$$E_1 \cdot t_1 \cdot \frac{d^2 u_1(x)}{dx^2} - \tau_a(x) = 0 \quad (11)$$

Since shear strain along the *intermediate element m* can be written as:

$$\gamma_m(x) = \frac{u_1(x)}{t_m} \quad (12)$$

and shear stress is equal to:

$$\tau_a(x) = G_m \cdot \frac{u_1(x)}{t_m} \quad (13)$$

Eq. (11) can be written as:

$$\frac{E_1 \cdot t_1 \cdot t_m}{G_m} \cdot \frac{d^2 \cdot \tau_a(x)}{dx^2} - \tau_a(x) = 0 \quad (14)$$

Finally, introducing a dimensional coefficient,  $\beta^2$ , equal to:

$$\beta^2 = \frac{G_m}{E_1 \cdot t_1 \cdot t_m} \quad (15)$$

Eq. (14) can be written as:

$$\frac{d^2 \cdot \tau_a(x)}{dx^2} - \beta^2 \cdot \tau_a(x) = 0 \quad (16)$$

The solution of Eq. (16) is given by the following function:

$$\tau_a(x) = \frac{P_1}{b_1} \cdot \beta \cdot \frac{\cosh(\beta x)}{\sinh(\beta L)} \quad (17)$$

The strain at the top of the *adherent I* may be expressed as:

$$\varepsilon_{1,top} \cong \frac{du_{1,a}}{dx} = \frac{du_1(x)}{dx} \quad (18)$$

Taking into account Eq. (13), is it possible to write:

$$\varepsilon_{1,top} = \frac{t_m}{G_m} \cdot \frac{P_1}{b_1} \cdot \beta^2 \cdot \frac{\sinh(\beta x)}{\sinh(\beta L)} \quad (19)$$

The maximum value of strain at the edge of the joint is:

$$\varepsilon_{1,top}(x = L) = \frac{t_m}{G_m} \cdot \frac{P_1}{b_1} \cdot \beta^2 \quad (20)$$

The elastic stage of deformation of the bonded joints ends when the shear stress reaches the local

shear strength  $\tau_{max}$  at the slip of  $u_{max}$ , for  $x=L$ , considering  $L$  as the maximum value of bond length; it is possible to write:

$$\tau_{max}(x = L) = \frac{P_1}{b_1} \cdot \beta \cdot ctgh(\beta L) \cong \frac{P_1}{b_1} \cdot \beta = \frac{P_1}{b_1} \cdot \sqrt{\frac{G_m}{E_1 \cdot t_1 \cdot t_m}} \quad (21)$$

Assuming the interfacial fracture energy value,  $G_f$ , as:

$$G_f = \frac{1}{2} \cdot \tau_{max} \cdot u_{max} = \frac{1}{2} \cdot \frac{t_m}{G_m} \cdot \tau_{max}^2 = \frac{P_1^2}{2 \cdot b_1^2 \cdot E_1 \cdot t_1} \quad (22)$$

the value of load capacity can be written as follows:

$$P_1 = b_1 \cdot \sqrt{2 \cdot E_1 \cdot t_1 \cdot G_f} \quad (23)$$

where  $G_f$  is the interfacial fracture energy i.e. the total external energy supply per unit of area, required to create and propagate delamination along the GFRP strip-to brickwork masonry bonded joint without taking into account the mortar layers in the masonry.

Comparison of theoretical values and experimental results allow confirming the availability of the bond analysis above.

### 3. EXPERIMENTAL ANALYSIS

#### 3.1. Specimens and set up for pull-push tests

In order to analyze the behavior of GFRP strip-to brickwork masonry joints two types of brickwork masonry have been adopted in the investigation, modern and historical brickwork masonry with different values of mortar bed joints. Handmade historic clay bricks from an ancient building were removed during restoration work and used to build masonry wallets; identical masonry wallets were built using modern full clay bricks.

The experimental program foresaw a series of preliminary tests on the materials adopted in the specimens: compressive tests on historic and modern bricks and wallets; tensile tests on GFRP strips. 21 wallets  $w_i$  with  $i=1, \dots, 3$  - index is referred to the thickness of mortar bed joints equal, respectively, to 4mm, 8mm and 12 mm - were prepared for the investigation; each one was made of



four bricks with bed mortar joints of different thicknesses. More precisely, 12 specimens were made using historic clay bricks and the other 8 were made using modern bricks. Four historic specimens and three modern ones were made for each of the mortar bed joint thicknesses.

Table 1 - Clay historic prisms from historic bricks under compressive tests

Clay prism*	Depth [mm]	Length [mm]	Height [mm]	Section A <sub>b</sub> [mm <sup>2</sup> ]	Load P <sub>u</sub> [kN]	Strength σ <sub>r</sub> [N/mm <sup>2</sup> ]
CR1	60	55	60	3300	159.084	48.21
CR2	60	56	60	3360	128.789	38.33
CR3	60.5	55	60.5	3327.5	130.531	39.23
CM1	60	57	60	3420	66.239	19.37
CM1	60	58	60	3480	75.738	21.76
CM1	60	59	60	3540	76.537	21.62
CG1	61	55	61	3355	65.892	19.64
CG2	60.5	55	61	3327.5	61.309	18.42
CG3	60.5	55	60.5	3327.5	76.883	23.10

\*prisms are classified basing on the percentage of iron in the composition of the clay:  
CR=high quantity of iron; CM=medium quantity of iron; CG=low quantity of iron.

Table 1 shows the dimensions of clay prisms from historic bricks (Figs. 2(a) and (b)), their failure load and their singular compressive strength. The average strength of clay prisms resulted:  $f_{b,av}=27.74 \text{ N/mm}^2$ . Table 2 shows the results of compressive tests done on modern clay prisms. The experimental results allow to evaluate a high strength of modern clay bricks with average strength resulted  $f_{b,av}=43.31 \text{ N/mm}^2$ .

Table 2 - Clay modern bricks subjected to compressive tests

Clay prism	Depth [mm]	Length [mm]	Height [mm]	Section A <sub>b</sub> [mm <sup>2</sup> ]	Load P <sub>u</sub> [kN]	Strength σ <sub>r</sub> [N/mm <sup>2</sup> ]
1	50.5	50.1	54.2	2530.05	90.92	35.93
2	50.9	50.9	55.5	2590.81	100.04	38.61
3	50.9	50.8	54.8	2585.72	144.33	55.82
4	50.7	50.1	54.4	2540.07	146.61	57.72
5	50.9	50.8	56.3	2585.72	110.6	42.77
6	50.2	50.1	56.7	2515.02	72.89	28.98

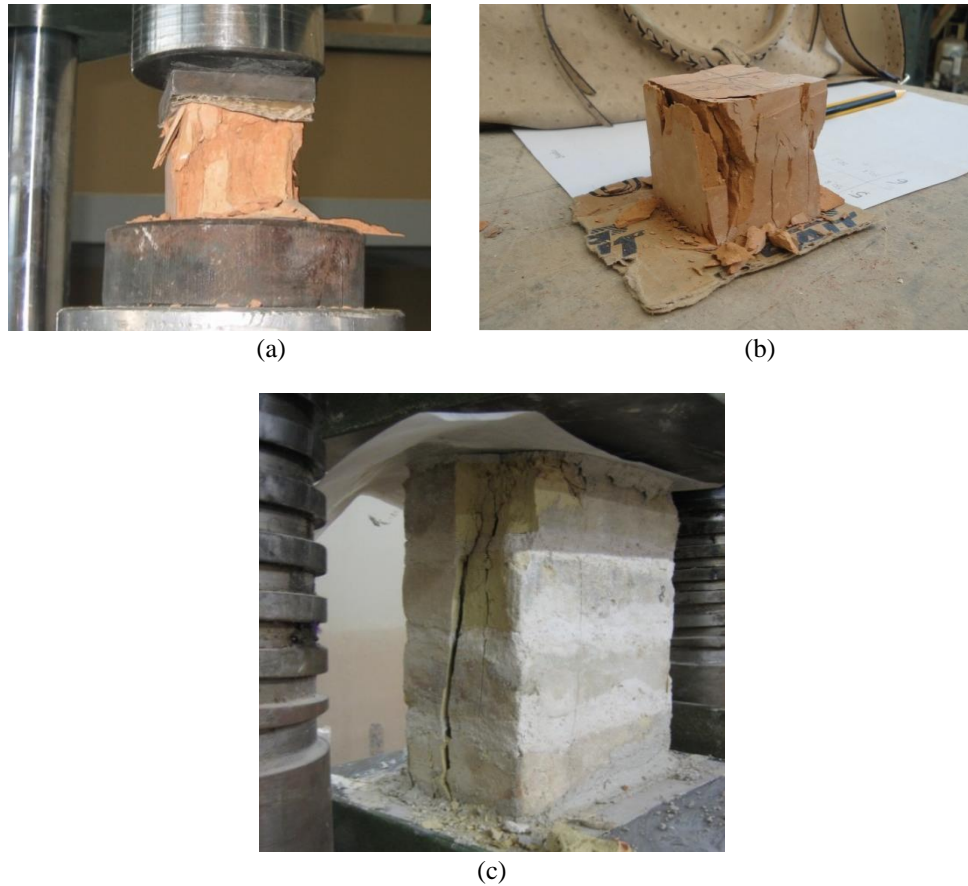


Figure 2 - (a) Compressive tests historic and (b) modern clay prisms; (c) compressive tests and view of failure of historic brickwork wallet.

Table 3 - Historical brickwork wallets under compressive tests

Wallet	Length [mm]	Width [mm]	Height [mm]	Thickness mortar joint [mm]	$A_b$ [ $10^3 \cdot \text{mm}^2$ ]	$P_u$ [kN]	Strength $\sigma_r$ [N/mm <sup>2</sup> ]	Average Strength $\sigma_{av.}$ [N/mm <sup>2</sup> ]
<b>W1D</b>	270	130	280	4.00	35.1	270	7.69	
<b>W2D</b>	270	130	292	8.00	35.1	355	10.11	<b>8.22</b>
<b>W3D</b>	270	130	294	12.00	35.1	241	6.86	

Table 4 - Modern brickwork wallets under compressive tests

Wallet	Length [mm]	Width [mm]	Height [mm]	Thickness mortar joint [mm]	$A_b$ [ $10^3 \cdot \text{mm}^2$ ]	$P_u$ [kN]	Strength $\sigma_r$ [N/mm <sup>2</sup> ]	Average Strength $\sigma_{av.}$ [N/mm <sup>2</sup> ]
<b>W1-C</b>	250	120	232	4.00	30.00	541.66	10.0553	
<b>W2-C</b>	250	120	244	8.00	30.00	358.59	11.953	<b>13.94</b>
<b>W3-C</b>	250	120	256	12.00	30.00	354.17	11.8057	

9 wallets made using historic clay bricks and 6 using modern bricks were reinforced by GFRP strips, and the other - three historic and two modern wallets - were subjected to compressive tests to evaluate the compressive strength of brickwork masonry (Fig. 2(c)). The mortar adopted in the

brickwork wallets was characterized by the following values of strength: average compressive strength  $f_{m,av}=12.1 \text{ N/mm}^2$  and bending tensile strength  $f_{m,t}=3.4 \text{ N/mm}^2$ . Tables 3 and 4 show geometrical data and results of compressive tests on historic and modern brickwork wallets with different mortar joints thicknesses subjected to compressive tests. As shown, the average compressive strength measured by tests was, respectively, equal to  $\sigma_{av}=8.22 \text{ N/mm}^2$  and to  $\sigma_{av}=13.94 \text{ N/mm}^2$  for historic brickwork masonry and modern masonry.

The wallets with EBS of GFRP strip were tested in the pull-push tests; the composite materials used were of the FIDGLASS UNIDIR 300 HS 73 type with the geometric and mechanical parameters shown in Table 5. In order to know the characteristics of GFRP, specimens were subjected to tensile tests [27]. Table 6 contains the results of tensile tests on GFRP specimens (Fig. 3).

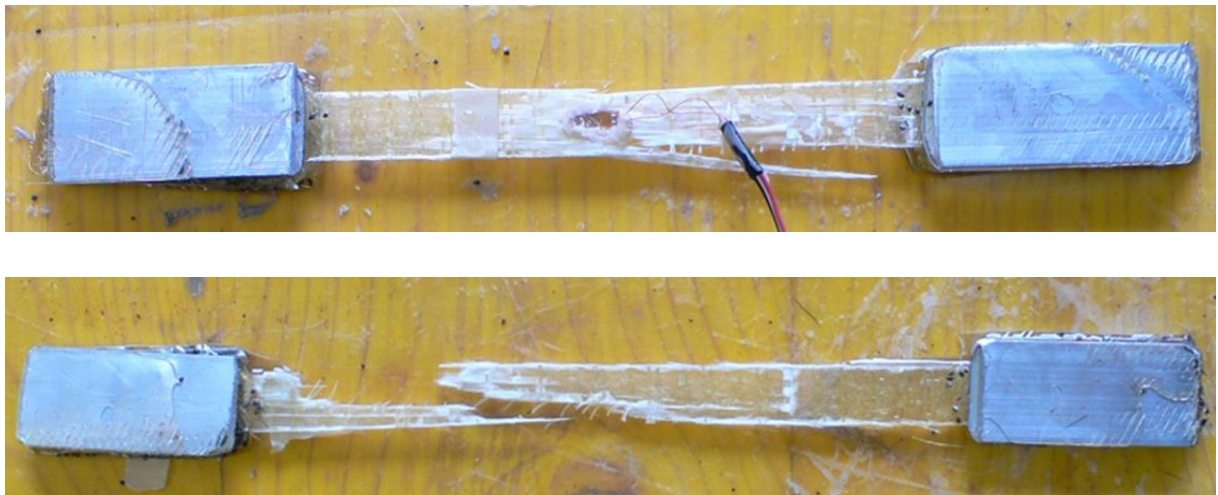


Figure 3 - Failure modes of GFRP specimens type AGM (Angled, Gage, Middle-ASTM D 3039) subjected to tensile tests.

Table 5 - Geometric and mechanical characteristics of the GFRP strip

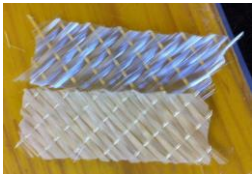
	Tensile strength	Young's Modulus	Ultimate strain	Thickness of strip	Density
	$f_{fk}$ [N/mm <sup>2</sup> ]	$E_1$ [N/mm <sup>2</sup> ]	$\varepsilon_f$ [%]	$t_1$ [mm]	$\rho$ [g/m <sup>2</sup> ]
<b>FIDGLASS UNIDIR 300 HS 73</b>	1400	70000	2.0	0.120	300

Table 6 - Experimental data of tensile tests on GFRP specimens.

Specimen	$P_{max}$ [N]	$A_f$ [mm <sup>2</sup> ]	$\sigma_{ft}$ [N/mm <sup>2</sup> ]	$E_{ft,exp.}$ [GPa]	Type of Rupture*
<b>G1</b>	6365	16.82	1229.524	-	AGM
<b>G2</b>	7169	18.45	1317.056	64,03	AGM

\*AGM=Angled, Gage, Middle –ASTM D 3039

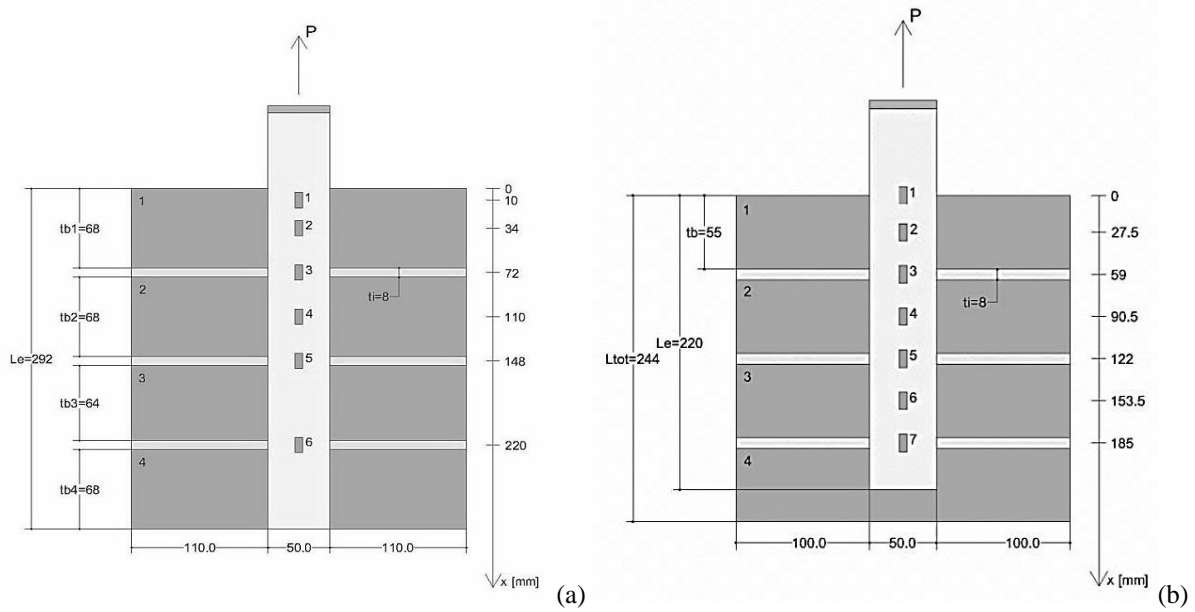


Figure 4 - Wallets with EBS GFRP strips and location of strain gauges: (a) in historic brickwork and (b) in modern brickwork.

The specimens were prepared with GFRP strips measuring 50mm in width, applied on the surfaces of the specimens, perpendicularly to the mortar layers. The application of EBS with GFRP strips on the brickwork surface foresaw: cleaning and smoothing the specimens' surface, the application of a bi-component primer (type MBACE PRIMER) on the surface of each specimen and using an epoxy resin (KIMITECH EP-IN) to glue the GFRP strips. The epoxy resin presented an average tensile strength equal to  $f_{res.}=30 \text{ N/mm}^2$  and Young's modulus  $E_{res.}=1760 \text{ N/mm}^2$ . For historic brickwork specimens the length of adhesion of the GFRP strip was equal to the length of the specimen in a range  $280\text{mm} \div 294\text{mm}$ : length of adhesion 280mm for specimens with 4mm of mortar layers; 292mm for the ones with 8mm of mortar layers and 294 for the ones with 12mm layers. For modern brickwork specimens, the length of adhesion of the GFRP strip was equal to 220 mm for all the specimen types (Figs. 4(a) and (b)). For the historic specimens, six strain gauges were located

on composite materials with different intervals due to both the different geometry of the historical clay bricks and, to the different thicknesses of the mortar layers. The strain gauges were placed in a univocal way in each specimen: the first one on the superior edge, the second in the middle of the first brick, the third in the middle of the first mortar layer, the fourth in the middle of the second brick, the fifth in the middle of the second mortar layer and, finally, the sixth strain gauge was placed in the middle of the third, and last, mortar layer. A scheme of the location of the strain gauges is shown in Figure 4(a). Seven strain gauges were used for the modern specimens as shown in Figure 4(b). The tests' set-up is shown in Figure 5: the specimens were fixed by an anchorage system made of steel plates and clamps inside a steel frame; the load was transferred to the GFRP strip which was connected to the load cell by a system of metallic plates. The instruments used in the tests were able to measure both vertical load with load-cells and the strains on the GFRP strips in a continuous manner.

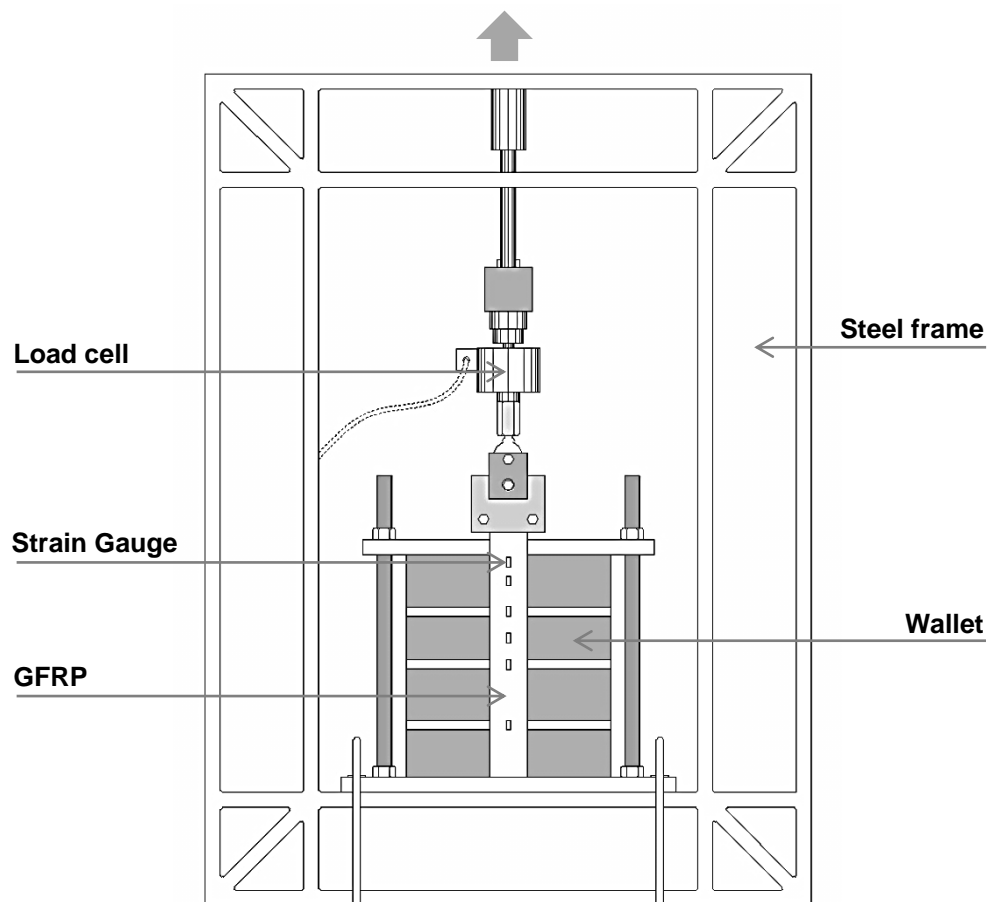


Figure 5 - Set up for pull-push shear tests: steel frame and blocking system for wallet.

### 3.2. Experimental results

The delamination of composite material as typical failure of EBS with GFRP strip-to-brickwork masonry bonded joints was recorded in many specimens even if it is at times accompanied by rupture of GFRP strips and bricks on the edge. In Figures 6(a), (b) and (c) typical delamination failure mode for historic brickwork specimens is shown: delamination of GFRP strip due to the detachment of a surface layer of brick with successive compressive failure of brick on the loaded edge. The mechanisms of failure are obviously influenced by the characteristics of strength, porosity, clay composition and mode of execution of historic bricks which are different although they were taken from the same building. Figures 7(a), (b) and (c) show the typical delamination failure for wallets made of modern bricks. It is possible to notice that, in this case, delamination of the GFRP strip did not cause the detachment of the surface layer of the specimen.

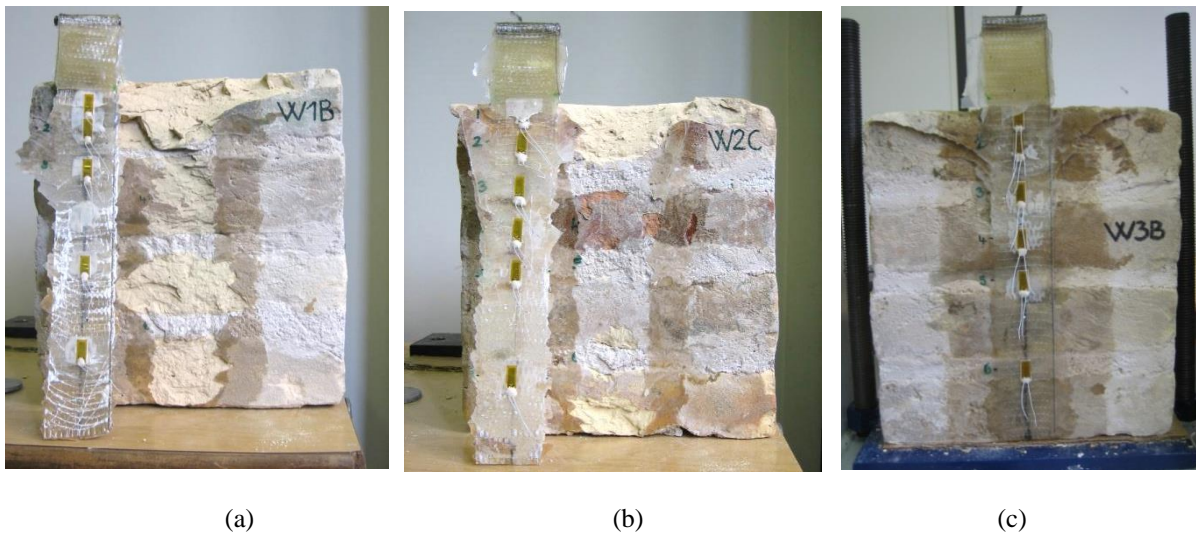


Figure 6 - Typical delamination failure of GFRP strip-to-historic-brickwork joint for wallets with different thickness of mortar joints: (a) thickness 4mm; (b) 8mm and (c) 12mm.

Table 7 contains the experimental failure loads of pull-push tests on the historic brickwork specimens. The average failure load value was  $P_u=8850\text{N}$  for specimen  $w_1$  with 4mm mortar layers,  $P_u=8280\text{N}$  for specimen  $w_2$  with 8mm mortar layers and  $P_u=8470\text{N}$  for specimen  $w_3$  with 12mm mortar layers. Hence, it is possible to affirm that, given that the values for the failure loads were very similar, there was no evident difference between the three kinds of wallets  $w_i$  with  $i=1,\dots,3$ .



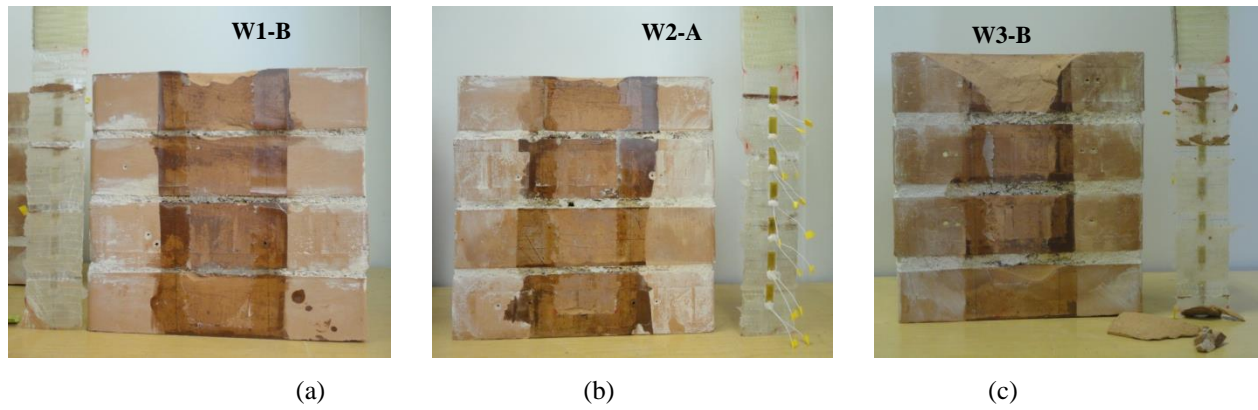


Figure 7 - Typical delamination failure of GFRP strip-to-modern-brickwork joint for wallets with different thickness of mortar joints: (a) thickness 4mm; (b) 8mm and (c) 12mm.

Table 7 - Exp. failure load, stress and type of failure for wallets with historic bricks.

Wallet	mortar layer h [mm]	Load $P_u$ [N]	Strength $\sigma_{f,max}$ [N/mm <sup>2</sup> ]	Mechanism of failure*
W1A	4.00	10735	1789	D+GFR
W1B	4.00	9632	1605	D
W1C	4.00	6179	1030	D+GFR
W2A	8.00	8107	1351	D+GFR
W2B	8.00	8875	1479	D+GFR
W2C	8.00	7854	1309	D
W3A	12.00	6395	1066	D+GFR
W3B	12.00	9485	1581	D
W3C	12.00	9532	1589	D+GFR

\*D=Delamination, D+GFR=Delamination + Glass-Fiber Rupture

Table 8 - Exp. failure load, stress and type of failure for wallets with modern bricks.

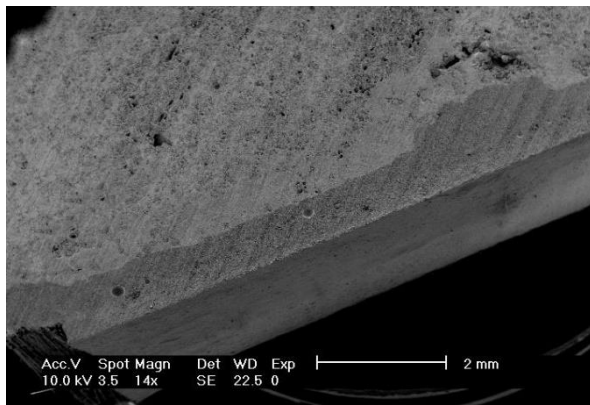
Wallet	mortar layer h [mm]	Load $P_u$ [N]	Strength $\sigma_{f,max}$ [N/mm <sup>2</sup> ]	Mechanism of failure*
W1-A	4.00	6298	1050	D
W1-B	4.00	7903	1317	D
W2-A	8.00	6296	1049	D
W2-B	8.00	7273	1212	D+GFR
W3-A	12.00	7345	1224	D+GFR
W3-B	12.00	6221	1037	D

\*D=Delamination, D+GFR=Delamination + Glass-Fiber Rupture

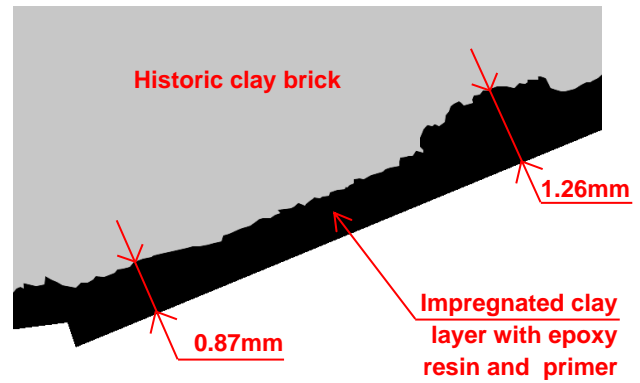
The experimental results obtained for the modern brickwork specimens are shown in Table 8: the average failure load was  $P_u=7100N$  for specimens  $w_1$ ,  $P_u=6784N$  for specimens  $w_2$ , and  $P_u=6783N$

for specimens w<sub>3</sub>; also in this case, it was possible to notice that there was no evident difference between the three kinds of specimens.

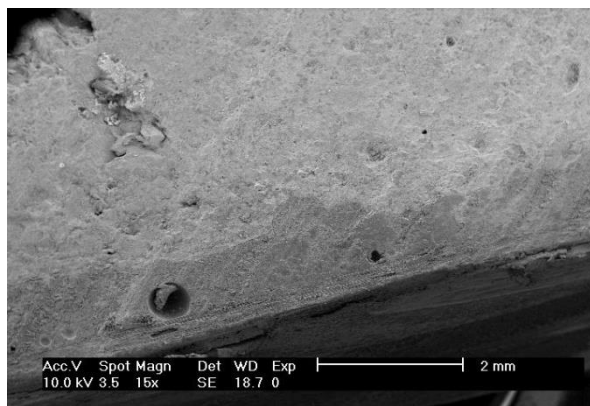
An in-depth analysis was developed on the specimens made of historic clay bricks to analyse mechanism of failure caused by delamination and GFRP rupture; small parts of the tested specimens were observed by an electronic microscope to evaluate the penetration of both the primer and the epoxy resin inside the masonry surface. Figures 8 (a),(b),(c) and (d) show that the thickness of the *intermediate layer* may be assumed to be equal to about 1.2mm.



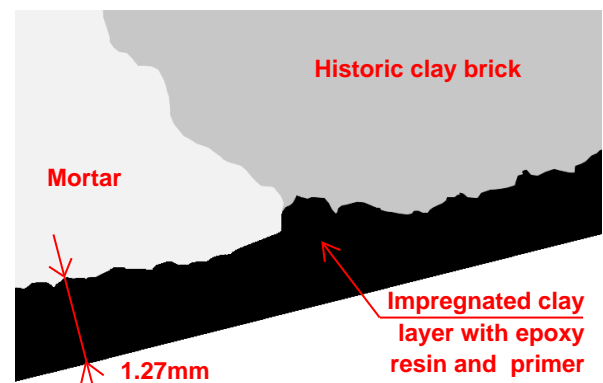
(a)



(b)



(c)



(d)

Figure 8 - Analysis by electronic microscope: (a) Impregnated clay layer and (b) with evaluation of thickness; (c), (d) clay brick surface and mortar layer of the historic wallet.

Strain values were recorded for the GFRP strip bonded to brickwork wallets under pull-push test at different value of load P until failure of joint. Strains recorded on the strips were measured until the ultimate loads; diagrams of strain values are shown in Figures 9-11 for historic masonry. Figures



12-14 show strain values recorded for wallets with modern bricks  $w_i$  with  $i=1,\dots,3$  during pull-push shear tests on the 6 specimens.

By observing the experimental diagrams of strain vs. length of GFRP strip, for both kinds of specimens, it is possible to understand the starting point of the delamination process. The detachment of GFRP strips from the support starts at the point where the diagram changes slope and continues until the complete detachment of the GFRP strip or its rupture.

Maximum strains, recorded during the tests, assumed a value equal to about  $\varepsilon = 7.5 \times 10^{-3}$  both for modern and historic masonry without relevant difference for different thicknesses of mortar joints.

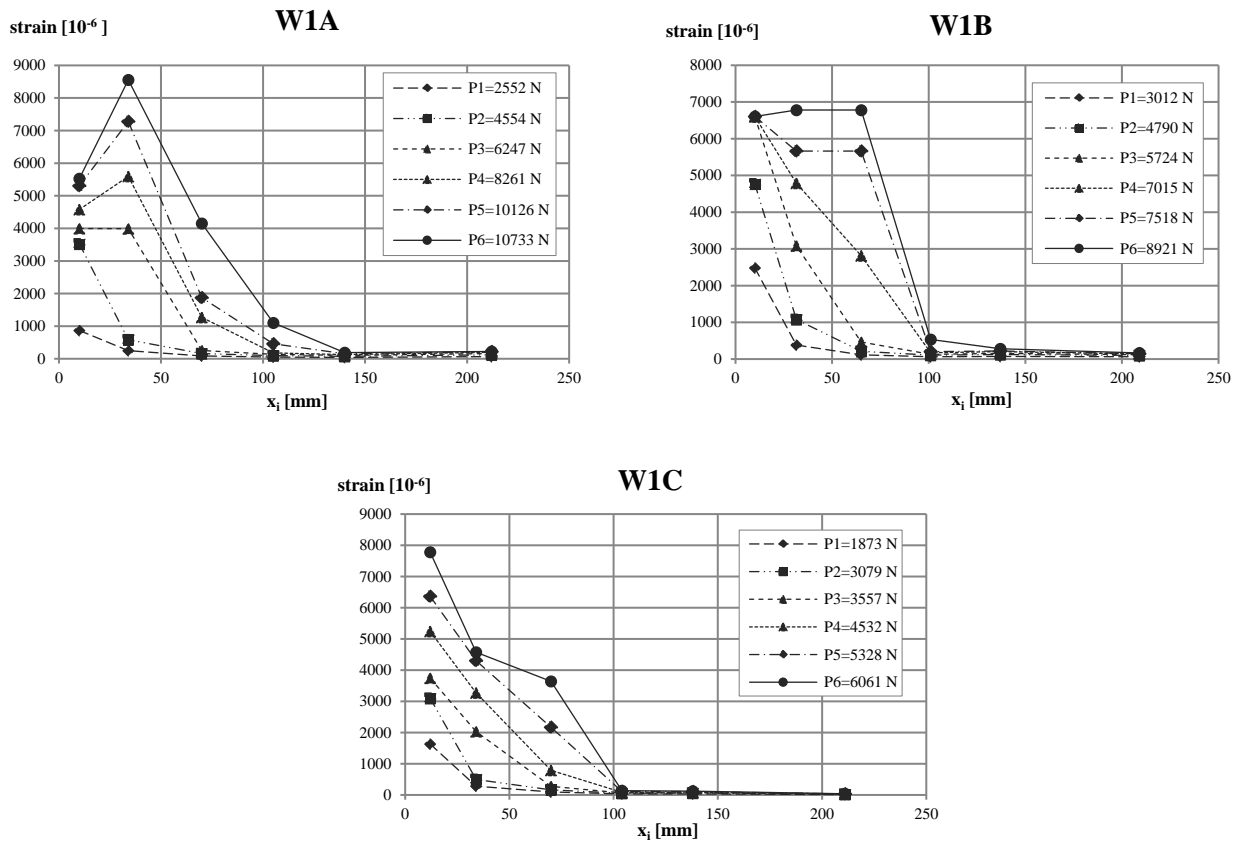


Figure 9 – Exp. strain values recorded for wallets with historic bricks and 4 mm of mortar layers.

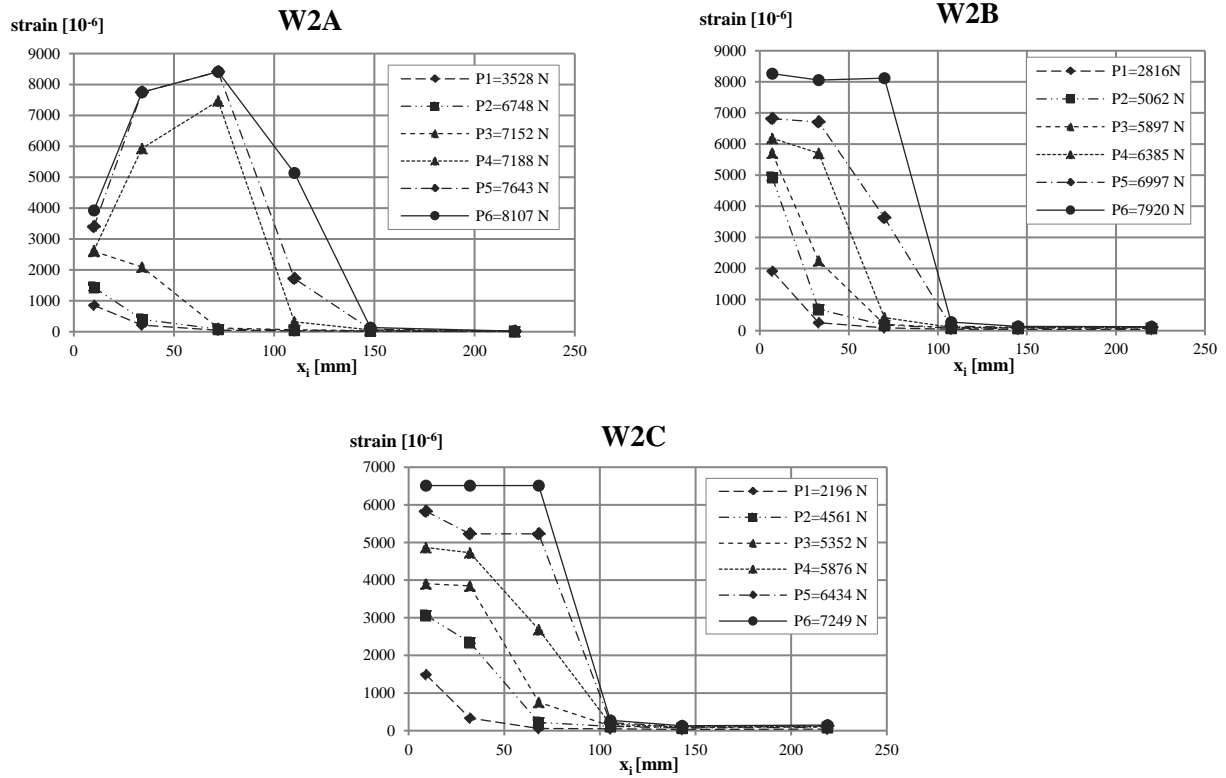


Figure 10 – Exp. strain values recorded for wallets with historic bricks and 8 mm of mortar layers.

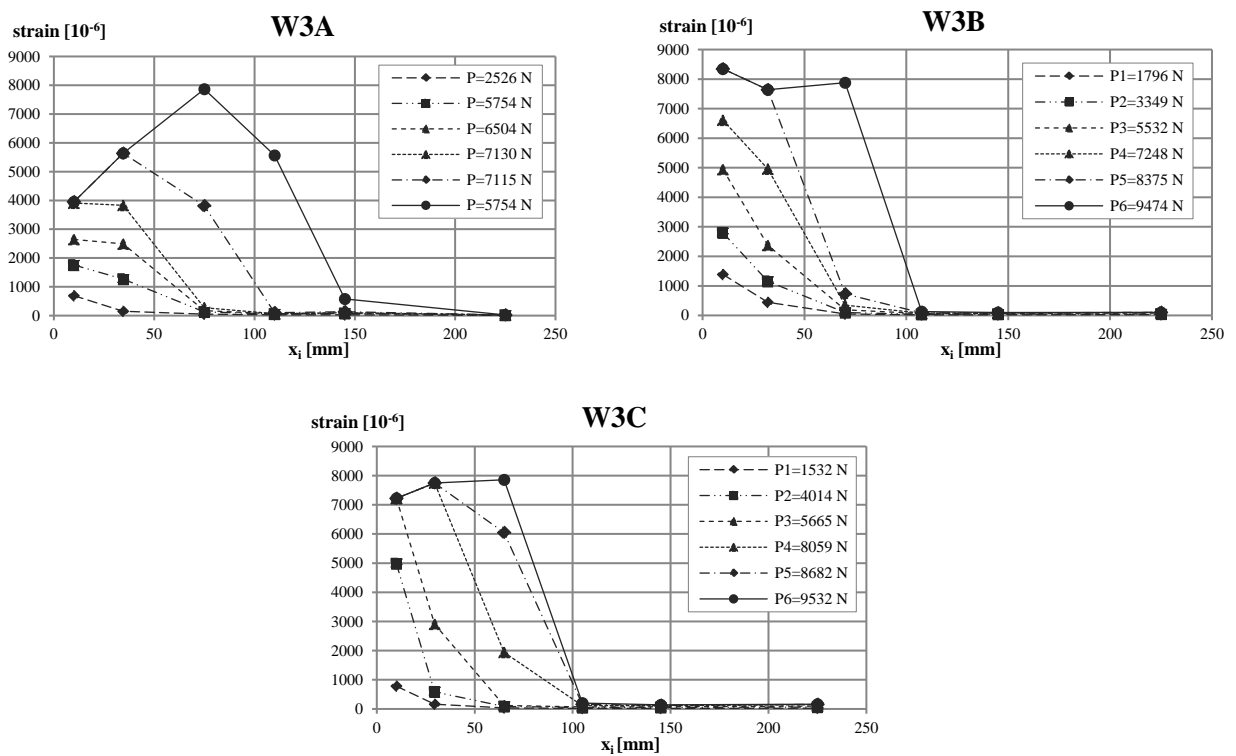


Figure 11 – Exp. strain values recorded for wallets with historic bricks and 12 mm of mortar layers.

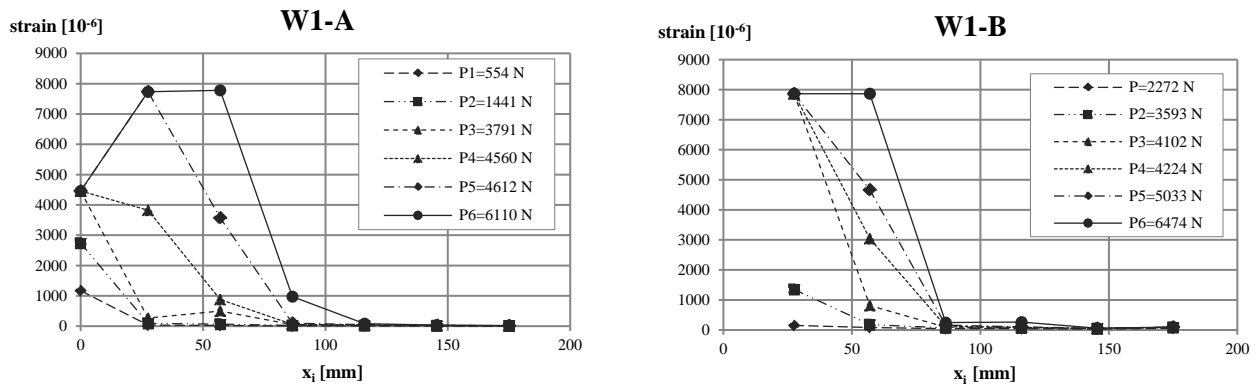


Figure 12 – Exp. strain values recorded for wallets with modern bricks and 4 mm of mortar layers.

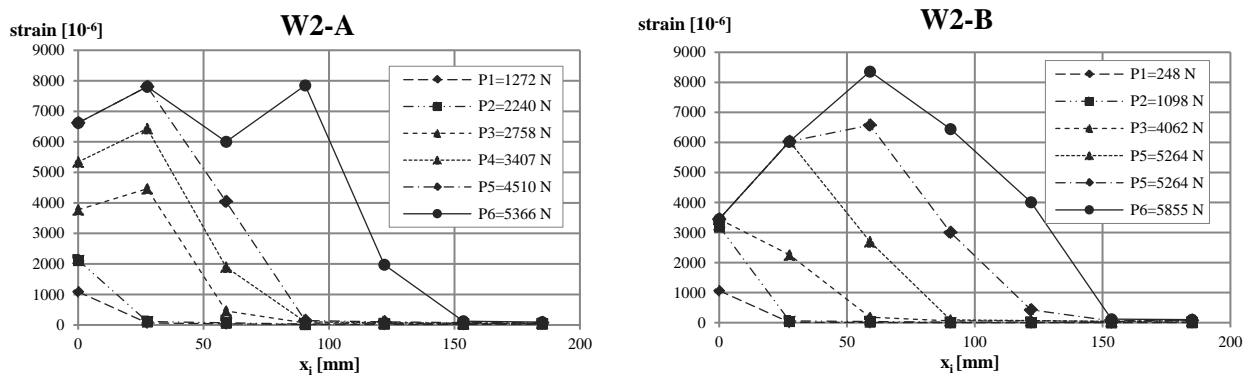


Figure 13 – Exp. strain values recorded for wallets with modern bricks and 8 mm of mortar layers.

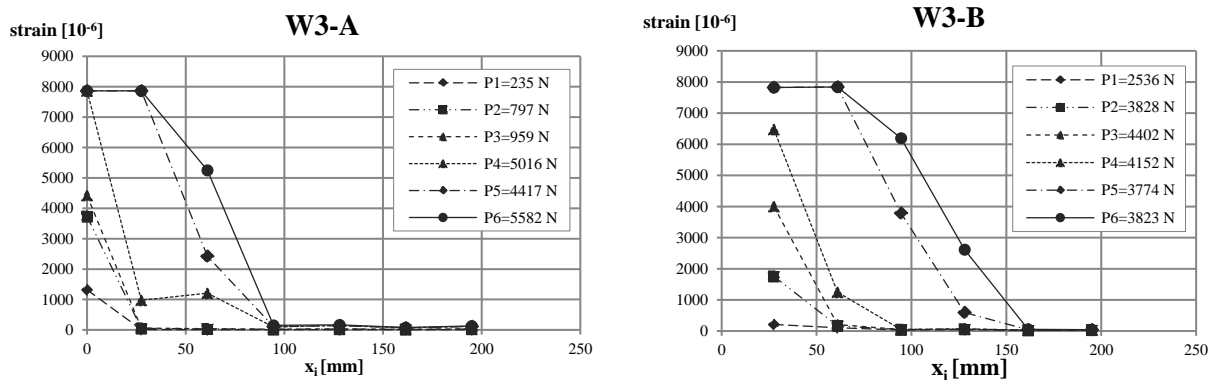


Figure 14 – Exp. strain values recorded for wallets with modern bricks and 12 mm of mortar layers.

### 3.3 Experimental shear stress-slip laws

The experimental results recorded during the pull-push shear tests on specimens were utilised to evaluate the functions shear stress and slip on the length  $L$  of adhesion surface; finally, the experimental interfacial laws,  $\tau - \delta$ , were determined. The theoretical procedure takes into account

that a number  $m$  of strain gauges is used to measure axial strains in FRP strips during the tests [18].

The position of strain gauges is indicated by  $x_i$ . For an interval  $\Delta x_i$  between the strain gauges, the following relation of the average shear stress value is:

$$\hat{\tau}_{i+1/2} = \frac{E_1 A_1 (\varepsilon_{i+1} - \varepsilon_i)}{b_1 (x_{i+1} - x_i)} \quad (24)$$

where:  $A_1$ = section area of GFRP strip. Then the integration of the strain profile starting from the end strain gauge at  $x=x_m$ , gives the following expression for the displacement at generic abscissa  $x$ , with  $x_i \leq x \leq x_{i+1}$ :

$$\begin{aligned} \delta(x) &= \delta(x_{i+1}) + \int_x^{x_{i+1}} \varepsilon(\zeta) d\zeta = (x_{i+1}) + \int_x^{x_{i+1}} \left[ \varepsilon_i + \left( \frac{\varepsilon_i - \varepsilon_{i+1}}{x_{i+1} - x_i} \right) \cdot (x_{i+1} - \zeta) \right] \cdot d\zeta \\ &= \delta(x_{i+1}) + \varepsilon_i (x_{i+1} - x) + \frac{1}{2} \cdot \left( \frac{\varepsilon_i - \varepsilon_{i+1}}{x_{i+1} - x_i} \right) \cdot (x_{i+1} - x)^2 \end{aligned} \quad (25)$$

with  $\delta(x_m) = 0$ . Finally, the average slip at the interval  $x_i, x_{i+1}$  is:

$$\delta_{i+1/2} = \frac{\delta(x_{i+1}) + \delta(x_i)}{2} \quad (26)$$

Figures 15 to 17 show experimental interfacial shear stress,  $\tau$ , vs. slip,  $\delta$ , diagrams for the tested specimens of historic brickwork wallets with EBS of GFRP strip evaluated for ultimate load value with different mortar joints. The maximum values of shear stress  $\tau_f$  and related slip  $\delta_f$  are indicated in the diagrams and values are in Table 9. Figures 18 to 20 show experimental interfacial shear stress,  $\tau$ , vs slip,  $\delta$ , diagrams for the tested specimens of modern brickwork wallets with EBS of GFRP strip evaluated with different mortar bed joint widths.

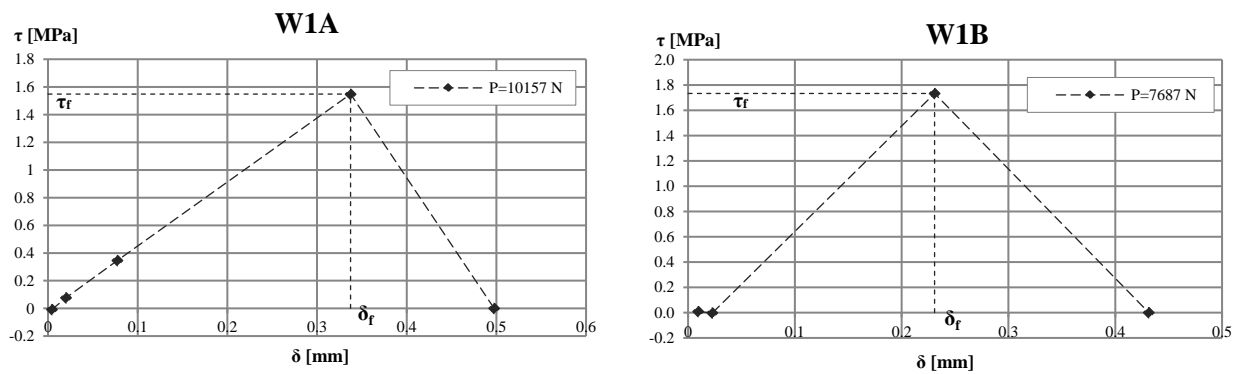


Figure 15 - Exp. interface diagram shear stress,  $\tau$ , vs slip,  $\delta$ , for tested historic brickwork wallets W1A-W1B with thickness of mortar joints equal to 4mm.

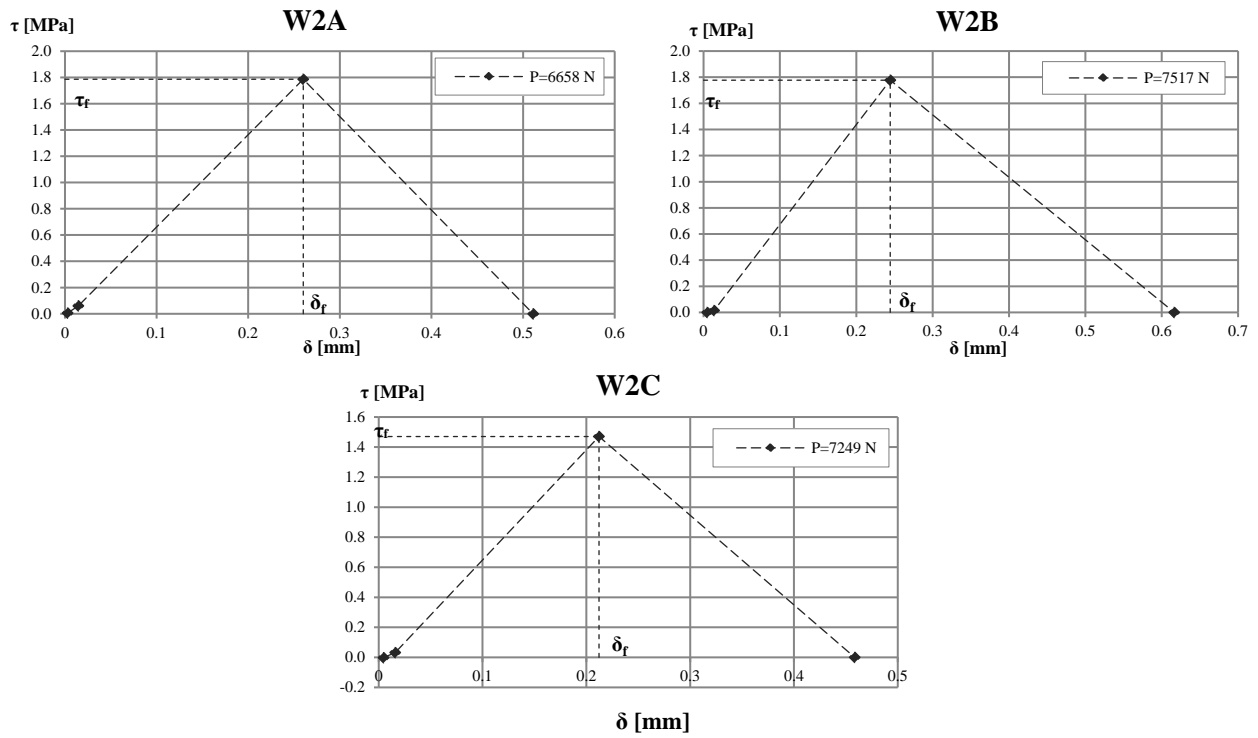


Figure 16 - Exp. interface diagram shear stress,  $\tau$ , vs slip,  $\delta$ , for tested historic brickwork wallets W2A-W2B-W2C with thickness of mortar joints equal to 8mm.

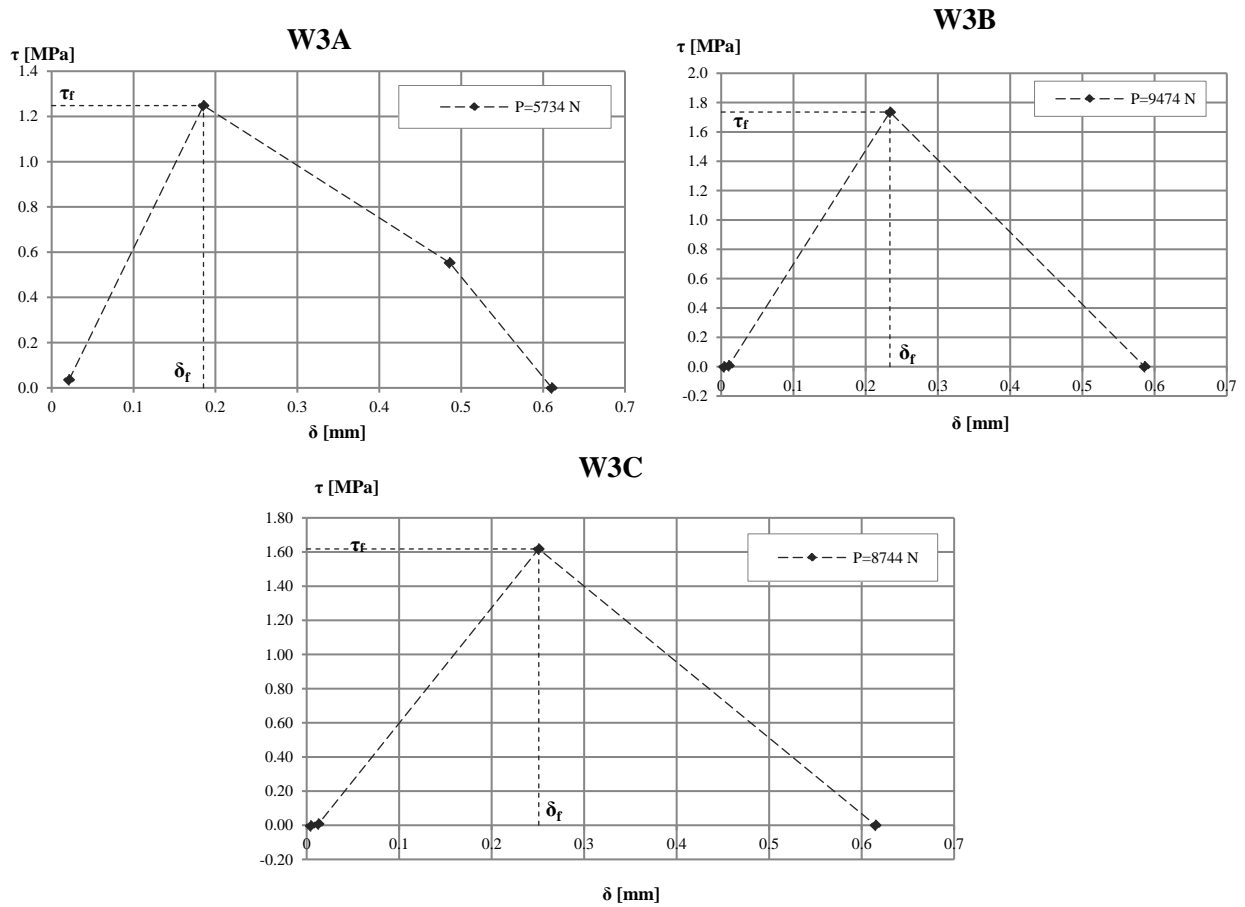


Figure 17 - Exp. interface diagram shear stress,  $\tau$ , vs slip,  $\delta$ , for tested historic brickwork wallets W3A-W3B-W3C with thickness of mortar joints equal to 12mm.

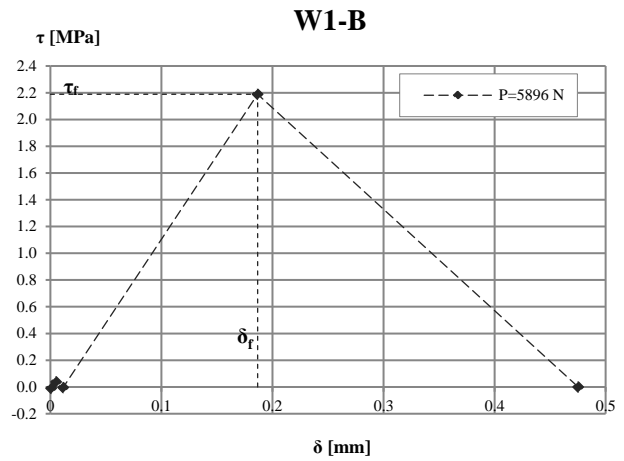
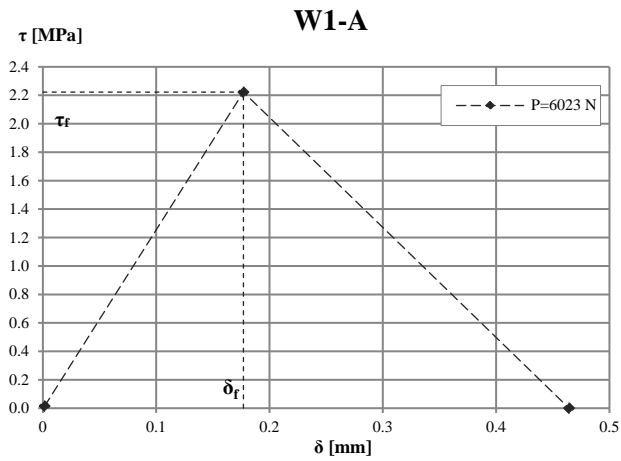


Figure 18 - Exp. interface diagram shear stress,  $\tau$ , vs slip,  $\delta$ , for tested modern brickwork wallets W1A-W1B with thickness of mortar joints equal to 4mm.

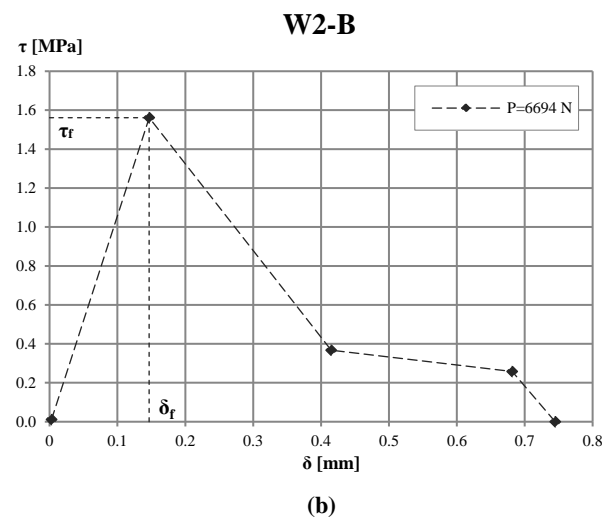
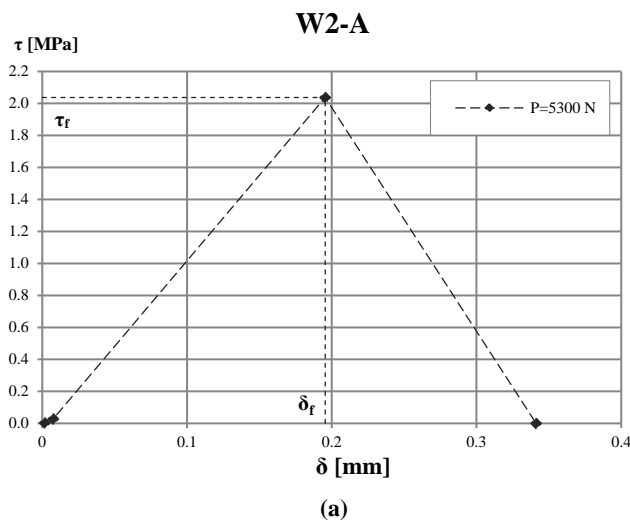


Figure 19 - Exp. interface diagram shear stress,  $\tau$ , vs slip,  $\delta$ , for tested modern brickwork wallets W2A-W2B with thickness of mortar joints equal to 8mm.

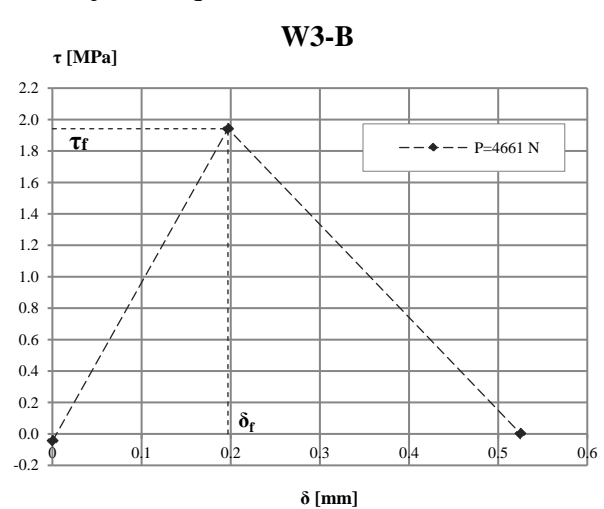
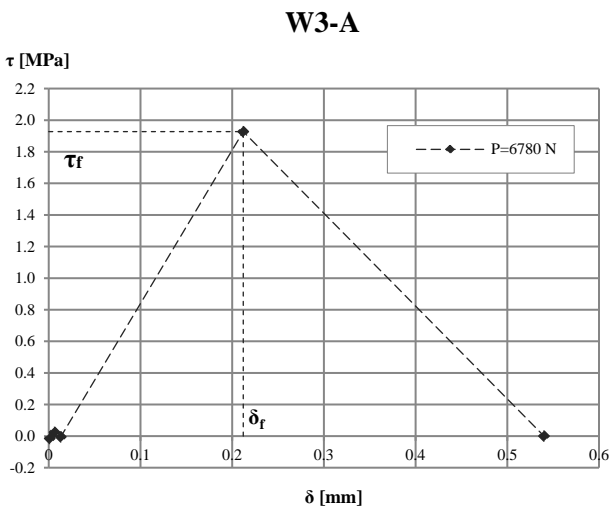


Figure 20 - Exp. interface diagram shear stress,  $\tau$ , vs slip,  $\delta$ , for tested modern brickwork wallets W3A-W3B with thickness of mortar joints equal to 12mm.

Table 9 – Exp. ultimate loads by pull-push test on historic-modern wallets and theor. ultimate load.

Brickwork wallets		Exp.ultimate load $P_u$ [N]	Fracture energy $G_f$ [N/mm]	Average values of $G_f^*$ [N/mm]	Slip $\delta_f$ [mm]	Shear stress $\tau_f$ [N/mm <sup>2</sup> ]	Theor. ultimate load $P_1$ [N]
Historic clay bricks	W1A	10157	0.383	0.332	0.337	1.548	4011
	W1B	7687	0.354		0.231	1.733	3856
	W1C	5341	0.258		0.404	1.311	3292
	W2A	6658	0.451	0.439	0.260	1.786	4352
	W2B	7517	0.537		0.244	1.777	4749
	W2C	7249	0.329		0.212	1.470	3717
	W3A	5734	0.411	0.467	0.185	1.248	4155
	W3B	9474	0.501		0.234	1.736	4587
	W3C	8744	0.488		0.251	1.618	4527
Modern clay bricks	W1-A	6023	0.516	0.512	0.177	2.222	4655
	W1-B	5896	0.508		0.187	2.189	4619
	W2-A	5300	0.343	0.403	0.195	2.037	3796
	W2-B	6694	0.463		0.147	1.561	4410
	W3-A	6780	0.507	0.507	0.212	1.927	4615
	W3-B	4661	0.506		0.197	1.942	4610

### 3.4. Discussion

In Table 9, ultimate load values both experimental,  $P_u$ , and theoretical,  $P_1$ , slip values  $\delta_f$ , maximum value of shear stress values,  $\tau_f$ , and, finally, fracture energy  $G_f$  are shown for both types of wallets subjected to pull-push shear tests. The ultimate value of  $P_1$  was determined by Eq. (23) and is compared with the experimental value. It can be noted that the theoretical values are lesser than the experimental values, obviously the appraisal theoretical analysis is linear elastic while the actual behaviour is non linear.

The experimental failure is characterised by mechanism of delamination; average values of slip are, respectively, equal to  $\delta_f=0.26\text{mm}$  for specimens with historic clay bricks and equal to  $\delta_f=0.18\text{mm}$  for specimens with modern clay bricks. The corresponding values of maximum shear stress assumed average values, respectively, equal to  $\tau_f=1.58\text{N/mm}^2$  for specimens with historic bricks and equal to  $\tau_f=1.97\text{ N/mm}^2$  for specimens with modern clay bricks. The average slip value in the case of GFRP strip-to-historic brickwork wallet joints is higher than modern wallets while the

average shear stress is lower. However, the experimental recorded values of ultimate slips are typical of this type of joint [18,22] characterized by a relatively low fracture energy between, respectively,  $G_f=0.258\div0.537\text{N/mm}$  for specimens made by historic clay bricks and  $G_f=0.343\div0.516\text{ N/mm}$  for specimens made of modern bricks. The influence due to the thickness of the bed mortar joints is quite limited on the fracture energy and, consequently, on the bond capacity of GFRP strips. Table 10 shows the comparison between experimental recorded strain values  $\varepsilon_{1,\text{top}}$  at loaded edge for ultimate load  $P_u$  and theoretical strain values evaluated with  $P_1$  obtained by Eq. (20) assuming the coefficient  $\beta^2$  from Eq. (15). Experimental average recorded strain is equal to about  $\varepsilon_{1,\text{top}}=7.7\cdot 10^{-3}$  for joints with historic wallets and  $7.32\cdot 10^{-3}$  with modern wallets.

Table 10 - Comparison between exp. and theor. strain values  $\varepsilon_{1,\text{top}}$

Brickwork wallets		Exp. strain $\varepsilon_{1,\text{top}}(x=L)$	Average exp. strain $\varepsilon_{1,\text{top}}\cdot 10^{-3}$	Theor. strain $\varepsilon_{1,\text{top}}(x=L)$	Average theor. strain $\varepsilon_{1,\text{top}}\cdot 10^{-3}$
Historic clay bricks	W1A	0.00856	7.65	0.00955	8.86
	W1B	0.00661		0.00918	
	W1C	0.00778		0.00784	
	W2A	0.00597	7.63	0.01036	10.17
	W2B	0.00826		0.01131	
	W2C	0.00687		0.00885	
	W3A	0.00787	7.81	0.00989	10.53
	W3B	0.00835		0.01092	
	W3C	0.00722		0.01078	
Modern clay bricks	W1-A	0.00774	7.80	0.01108	11.04
	W1-B	0.00787		0.01099	
	W2-A	0.00662	6.33	0.00904	9.77
	W2-B	0.00603		0.01050	
	W3-A	0.00786	7.84	0.01099	10.99
	W3-B	0.00782		0.01098	



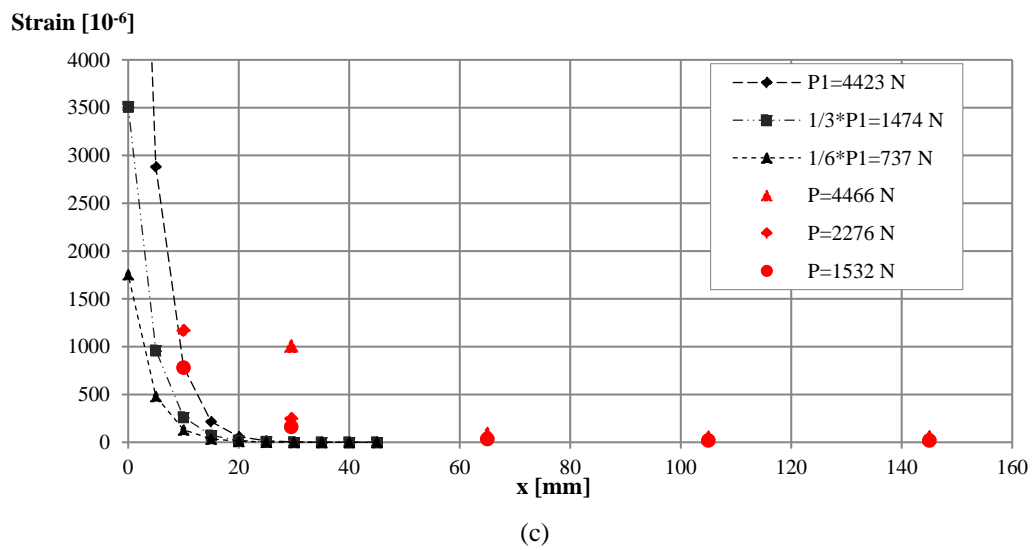
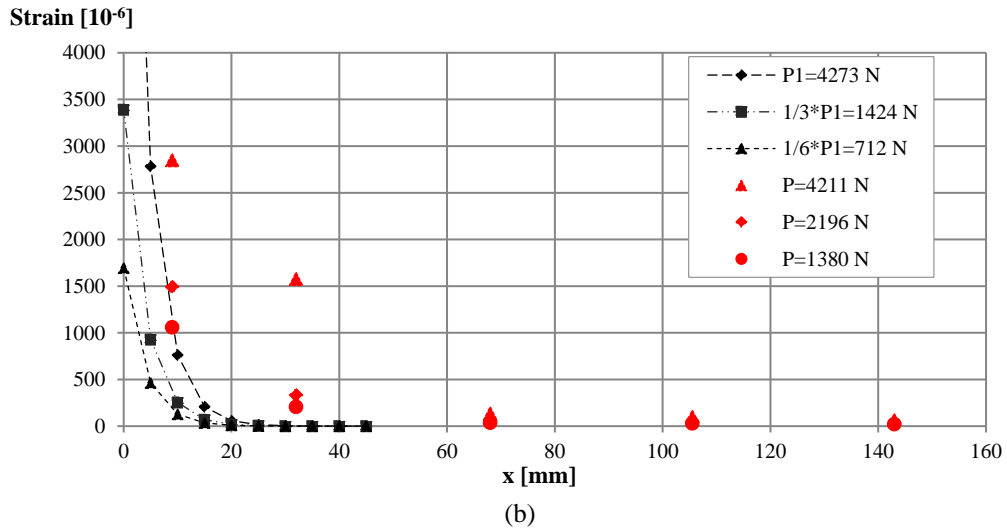
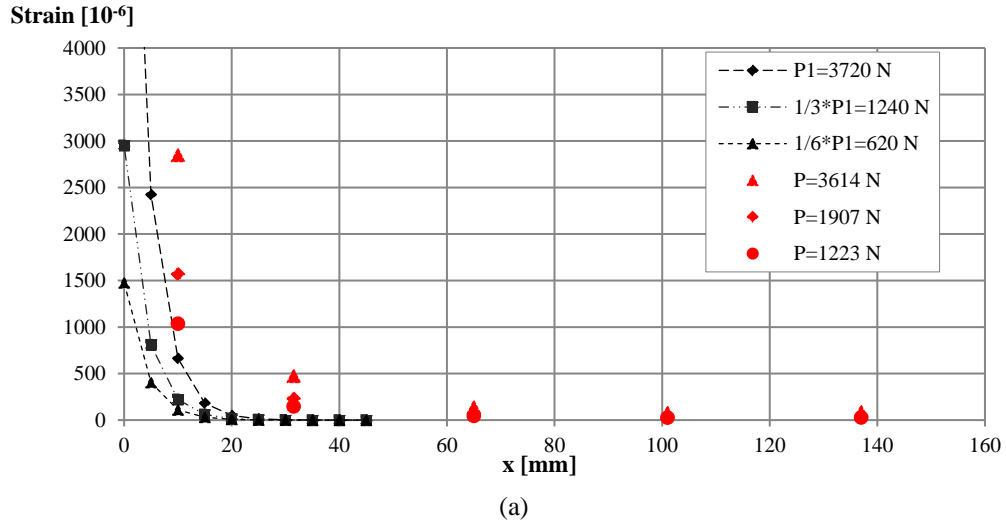


Figure 21 - Comparison between exp. and theor. strains for different loads on edge of GFRP-to-brickwork historic masonry wallets: (a) thickness 4mm (b) 8mm (c) 12mm of mortar joints.

Figure 21 shows comparison of strain  $\varepsilon(x)$  versus length of adhesion (maximum value equal to 70mm from the loaded edge) of GFRP-to-brickwork historic masonry wallets evaluated both by theoretical model and experimental tests. It may be noted that for theoretical values of load lesser than experimental  $P_u$ , the results are sufficiently close to experimental data. Figure 22 shows the comparison of strain once again evaluated both by theoretical model and experimental tests for the border length of 24mm of GFRP-to-brickwork modern masonry joints. The theoretical values of strains may be confrontable with experimental results obtained from tests in this case also.

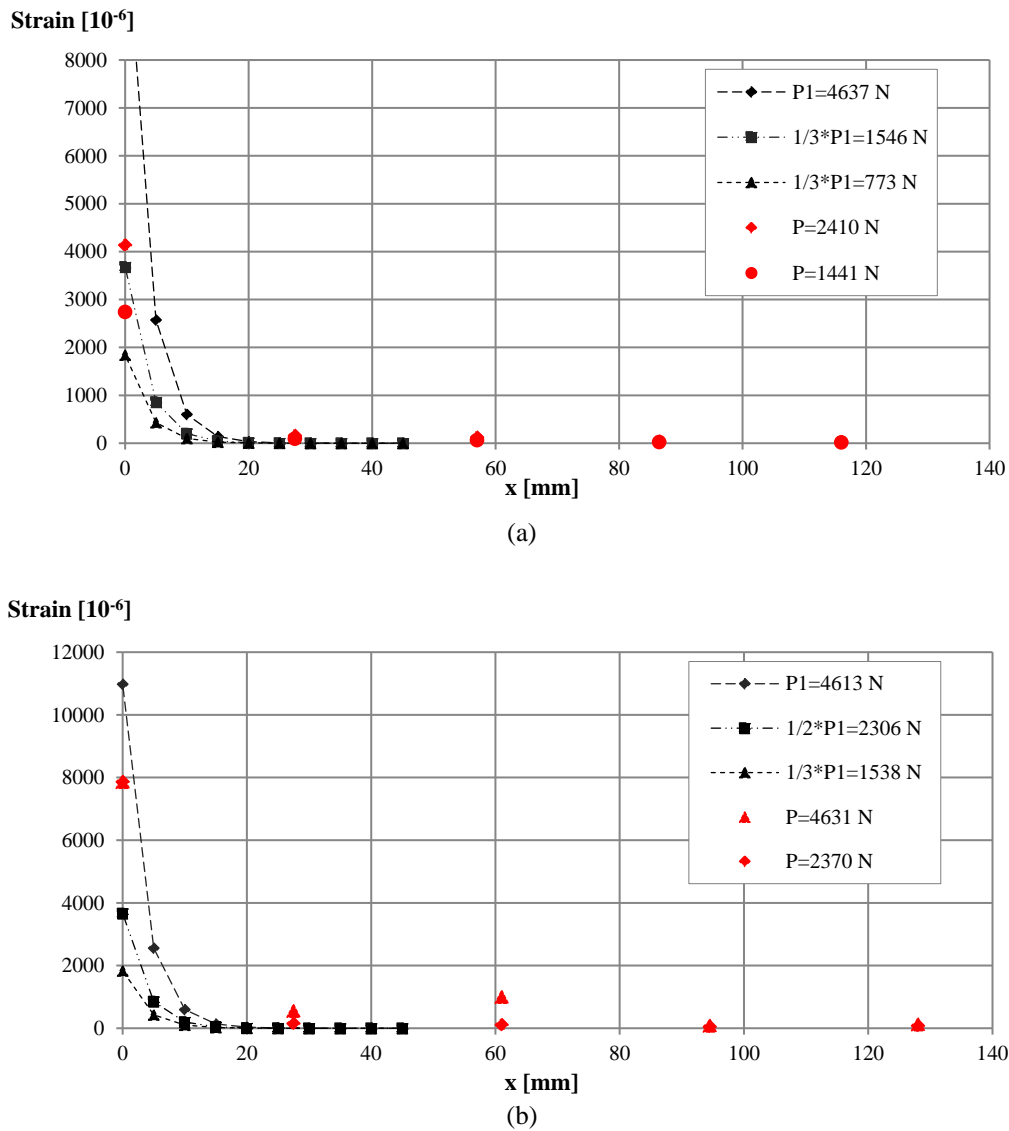


Figure 22 - Comparison between exp. and theor. strains for different loads on edge of GFRP-to-brickwork modern masonry wallets: (a) thickness 4mm (b) 12mm of mortar joints.

#### **4. CONCLUSIONS**

The shear behaviour of GFRP to-modern and historic brickwork masonry bonded joints and delamination failure were investigated experimentally in laboratory by pull-push shear tests. The following conclusions can be drawn from the experimental results:

- experimental tests confirmed that composite materials to historic brick bonded joints lose their capacity by brittle delamination failure;
- failure delamination is due to a relatively low fracture energy value varying between  $G_f = 0.258 \div 0.537$  N/mm for specimens made of historic clay bricks and  $G_f = 0.343 \div 0.516$  N/mm for specimens made of modern bricks;
- maximum ultimate shear stress  $\tau_f$  equal to  $2.22 \text{ N/mm}^2$  was recorded for GFRP to-modern brickwork masonry bonded joints with thickness of mortar equal to 4mm; instead maximum slip values  $\delta = 0.262 \text{ mm}$  was recorded in the case of historic wallets;
- bed mortar layers do not influence the delamination behavior since the values of fracture energy are heterogeneous notwithstanding their different thicknesses;
- the mechanism of delamination failure – especially in the case of GFRP to-historic brickwork masonry bonded joints is influenced by the weakness of masonry, although the support guarantees adhesion and higher values of ultimate slip ;
- a comparison between theoretical and experimental values confirms that adequate results may be obtained with appraisal of theoretical linear analysis.

#### **Acknowledgement**

This research was supported by research funds of University Politecnica delle Marche. The author would like to express his gratitude to the undergraduate students, doctoral students and technicians who collaborated in the development of the experimental tests.

## References

1. Triantafillou T.C. Strengthening of masonry structures using epoxy bonded FRP laminates. *Journal Composites for Construction*, 1998, **2**(5):96-104.
2. Shrive N.G. The use of fibre reinforced polymers to improve seismic resistance of masonry. *Const. and B. Mat.*, 2006, **20**: 269-277.
3. Corradi M., Borri A., Vignoli A. Strengthening techniques tested on masonry structures struck by the Umbrian-Marche earthquake of 1997-199. *Const. and B. Mat.*, 2002, **16** (4): 229-239.
4. Ascione L., Feo L., Fraternali F. Load carrying capacity of 2D FRP/strengthened masonry structures. *Composites*, 2005, **36**: 619-626.
5. Valluzzi M.R., Tinazzi D., Modena C. Shear behaviour of masonry panels strengthened by FRP laminates. *Const. and B. Mat.*, 2002, **16**: 409-416.
6. Capozucca R. Experimental analysis of historic masonry walls reinforced by CFRP under in-plane cyclic loading. *Composite Structures*, 2011, **94**: 277-289.
7. CNR-DT 200 R1/2012. Guide for the Design and Construction of Externally Bonded FRP systems for Strengthening. Council of National Research, Rome, 2012 (in English).
8. Teng J.G., Chen J.F., Smith S.T., Lam L. FRP strengthened RC structures. 2002, J. Wiley & Sons, England.
9. Chen J.F., Teng J.G. Anchorage strength models for FRP and steel plates bonded to concrete. *J. Structural Eng.*, ASCE, 2001; **127** (7): 784-791.
10. Wu Z., Yuan H., Niu H. Stress transfer and fracture propagation in different kind of adhesive joints. *J. of Eng. Mechanics*, 2002, **128** (5): 562-573.
11. Yuan H., Teng J.G., Seracino R. Wu Z.S., Yao J. Full-range behavior of FRP-to-concrete bonded joints. *Engineering Structures*, 2004, **26**: 553-565.
12. Pan J., Wu Y.F. Analytical modeling of bond behavior between FRP plate and concrete. *Composites: Part B*, 2014, **61**: 17-25.

13. Cosenza E., Manfredi G., Realfonzo R. Analytical modeling of bond between FRP reinforcing bars and concrete. Proc. Non Metallic (FRP) Reinforcement for Concrete Structures. 1995; Edited by L. Taerwe. RILEM.
14. Wang J. Debonding of FRP-plated reinforced concrete beam, a bond-slip analysis. I. Theoretical formulation. Int. Journal of Solids and Structures, 2006, **46**: 6649-6664.
15. Da Silva L.F.M., Das Neves P.J.C., Adams R.D., Spelt J.K. Analytical models of adhesively bonded joints. Part I: literature survey. Int. Journal of Adhesion & Adhesive, 2009, **29**: 319-30.
16. Da Silva L.F.M., Das Neves P.J.C., Adams R.D., Spelt J.K. Analytical models of adhesively bonded joints. Part II: Comparative study. Int. J. of Adhesion & Adhesive, 2009, **29**: 331-41.
17. Ferracuti B., Savoia M., Mazzotti C. Interface law for FRP-concrete delamination. Composite Structures, 2007, **80**, 523-531.
18. Capozucca R. Experimental FRP/SRP-historic masonry delamination. Composite Structures, 2010, **92**: 891-903.
19. Aiello M.A., Sciolti M.S. Analysis of bond performance between FRP sheets and calcarenite stones under service and ultimate conditions. *Masonry International*, 2008, **21** (1): 15-28.
20. Ceroni F., Garofano A., Pecce M. Bond tests on tuff elements externally bonded with FRP materials. Materials and Structures, 2014, **48**(7). DOI:10.1617/s11527-014-0295-6.
21. Oliveira, D.V., Basilio I., Lourenço P.B. Experimental bond behavior of FRP sheets glued on brick masonry. *J. of Composites for Construction*, 2011, **15** (32).
22. Capozucca R. Effects of mortar layers in the delamination of GFRP bonded to historic masonry. Composites: Part B, 2013, **44**: 639-649.
23. Fedeles R., Milani G. Three-dimensional effects induced by FRP-from-masonry delamination *Composite Structures*, 2011, **93** (7) :1819-1831
24. Fedeles R., Milani G. A numerical insight into the response of masonry reinforced by FRP strips. The case of perfect adhesion. *Composite Structures*, 2010, 92(10): 2345-2357.

25. Tsai M.Y., Morton J. The effect of a spew fillet on adhesive stress distributions in laminated composite single-lap joints. *Composite Structures*, 1995, **32**: 123-131.
26. Tsai M.Y., Oplinger D.W., Morton J. Improved theoretical solutions for adhesive lap joints. *Int. Journal Solids Structures*, 1998, **35** (12): 1163-1185.
27. ASTM D 3039/D3039M-08. Tensile Properties of Polymer Matrix Composite Materials, in *Annual Book of ASTM: Composite Materials*; 2008.

### Notation

- $1, 2$  : index of adherent 1 and adherent 2
- $exp, theor$  : index for experimental value; index for theoretical value
- $b_m, t_m$  : width and thickness of ideal intermediate element
- $E_m, G_m$  : Young's modulus, shear modulus of ideal intermediate element
- $\gamma_m, \tau_a$  : shear strain of ideal intermediate element and constant shear stress
- $\beta$  : coefficient
- $E_l, G_l$  : Young's modulus, shear modulus of composite material
- $\varepsilon_l, \gamma_l$  : linear strain and shear strain
- $\sigma_l, \tau_l$  : axial stress and shear stress in composite material
- $f_b, f_{b,av}$  : compressive and average strength of clay brick
- $f_m, f_{m,av}$  : compressive and average strength of mortar
- $f_{res}$  : tensile strength of epoxy resin
- $E_{res}$  : Young's modulus of epoxy resin
- $\tau, \tau_f$  : shear stress and maximum value of shear stress
- $\delta, \delta_f$  : interfacial slip and maximum value of interfacial slip
- $G_f$  : fracture energy
- $P, P_u$  : exp. load in the GFRP strip bonded to brickwork masonry and ultimate load
- $P_1$  : maximum load